Inorganic Chemistry

Article

pubs.acs.org/IC

Is Higher Ratio of Monoclinic to Tetragonal in $LaVO_4$ a Better Luminescence Host? Redispersion and Polymer Film Formation

Reena Okram,[†] Ningombam Yaiphaba,[§] Raghumani Singh Ningthoujam,*[,⊥] and Nongmaithem Rajmuhon Singh*[,†]

[†]Department of Chemistry, Manipur University, Imphal-795003, India

[§]Department of Chemistry, D. M. College of Science, Imphal-795001, India

[⊥]Chemistry Division, Bhabha Atomic Research Center, Mumbai-400085, India

Supporting Information

ABSTRACT: Crystalline $LaVO_4:Eu^{3+}$ nanophosphors (NPs) codoped with metal ions (M^{n+} = Li^+, Sr^{2+}, and Bi^{3+}) are prepared in ethylene glycol (EG) medium at temperature ~140 °C in 3 h. A mixture of monoclinic and tetragonal phases is observed. The ratio of tetragonal to monoclinic phases increases with increase of Li^+ and Sr^{2+} concentration, but this is opposite in case of Bi^{3+} concentration. Lattice expansion occurs in the case of Li^+ and Sr^{2+} codoping. Li^+ ions occupy the interstitial sites instead of La^{3+} sites. Lattice contraction occurs in case of Bi^{3+} codoping indicating substitution of La^{3+} sites. Luminescence intensity is improved by codoping of M^{n+} irrespective of crystal structure. Charges of Li^+ and Sr^{2+} are different from that of La^{3+} (host lattice), whereas the charge of Bi^{3+} is same as that of La^{3+}. One interesting observation is in magnetic dipole transition that the intensity of the peak at 594 nm is more than that at 587 nm in the case of charge imbalance, whereas the reverse occurs in the case of charge balance. $LaVO_4:Eu^{3+}$ nanophosphors prepared in water medium have more luminescence intensity when compared to those prepared in ethylene glycol, and this is related to variation of ratio of tetragonal to monoclinic phases. The luminescence intensity is also enhanced as annealing temperature increases from 600 to 800 °C due to the improved crystallinity. Lifetime data are analyzed on the basis of exponential and nonexponential decay equations. Samples are dispersible in polar medium due to capping of particles by EG. Polymer films are prepared by dispersion of NPs in poly(vinyl alcohol), and extra borax is added in order to make cross-link between polymer molecules. Samples of NPs in the forms of powder, dispersion in liquid medium, and film show the red emission.

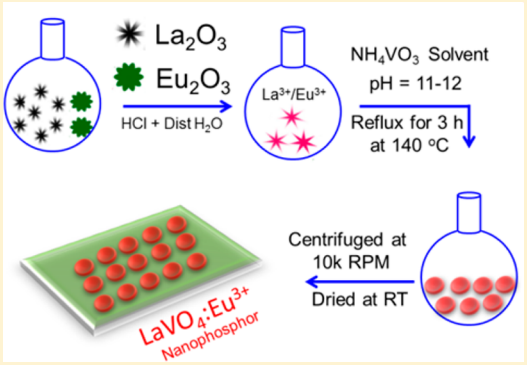

1. INTRODUCTION

Lanthanide orthovanadates ($LnVO_4$) are an important class of rare earth compounds that possess unique electronic, optical, and chemical characteristics along with numerous transition modes involving the 4f shell of rare earth ions. Therefore, they have been extensively used as phosphors,[1,2] polarizers,[3,4] laser host materials,[5,6] and catalysts.[7] Recent studies also disclose their potential application in biological detection and biotechnology.[8] All these have generated an impressive momentum for research on lanthanide orthovanadates in terms of synthesis, size, and structure-dependent luminescence behavior.[9−13]

Among $LnVO_4$ species, the $LaVO_4$ crystallizes in two polymorphs: monoclinic (*m*-) monazite type (space group: $P2_1/n$) and tetragonal (*t*-) zircon type (space group: $I4_1/amd$). Generally, with increasing ionic radius, Ln^{3+} ions show a strong tendency toward monazite structured orthovanadate owing to its higher oxygen coordination number (CN) of 9 as compared with 8 CN of the zircon type. La^{3+} ion, having the largest ionic radius of all the lanthanide ions, crystallizes solely in the monazite type as the thermodynamically stable state while other lanthanide orthovanadates prefer to crystallize in the zircon type. Zircon structure is composed of alternating edge-sharing AO_8 (A = trivalent atom) dodecahedra and VO_4 tetrahedra forming chains parallel to the *c*-axis, while in the monazite structure AO_9 polyhedra are edge-shared with VO_4 tetrahedra along the *c*-axis. Monazite $LaVO_4$ is not a suitable host for luminescent activators[14,15] compared to other lanthanum orthovanadate phases (say tetragonal (*t*-)). On the other hand, *t*-$LaVO_4$ is expected to have superior properties.[16] In *t*-$LaVO_4:Eu^{3+}$, for each vanadium or europium center, there are four bond bridges of La/Eu−O−V with a maximum angle of 153° making the σ-bonding overlap efficiently; thus, the energy transfer is greatly improved. In the case of *m*-$LaVO_4:Eu^{3+}$, the presence of only one La/Eu−O−V bond bridges and the other small bond bridge angles drastically reduced the possibilities of exchange interaction, making it hard

Received: February 12, 2014
Published: June 25, 2014

   dx.doi.org/10.1021/ic500828s | *Inorg. Chem.* 2014, 53, 7204−7213

for efficient energy transfer to occur. Therefore, structural transformation from monazite to tetragonal $LaVO_4$ can remarkably enhance the emission intensity of $LaVO_4$:Eu^{3+} phosphors.[17] In $LnPO_4$:Eu^{3+}, there are reports on enhancement in luminescence when crystalline phase changes from hexagonal to monoclinic or tetragonal.[18−20] Also, doping of appropriate amount of sensitizer so that energy transfer is possible to the activators (Ln^{3+}) serves to improve luminescence intensity. A sensitizer absorbs energy strongly, and subsequently, the absorbed energy is transferred to the excited states of the activator.

Eu^{3+} ion doped $LaVO_4$ has been chosen mainly because of its deviant luminescent behavior compared with other rare earth vanadates. From a standpoint of materials chemistry and physics, Eu^{3+} ion activated monazite and zircon type $LaVO_4$ represent interesting systems to test and develop fundamental ideas about synthesis and properties of doped nanomaterials. In our previous work,[21] we have synthesized *m*-$LaVO_4$:Eu^{3+} nanophosphors (NPs) by an ethylene glycol (EG) route at a relatively low temperature of 140 °C and have studied its luminescence properties in detail. A schematic diagram for the preparation of $LaVO_4$:Eu^{3+} NPs is shown in Figure 1.

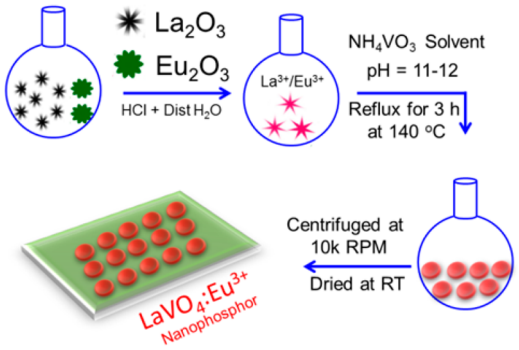

Figure 1. Schematic diagram showing the experimental process for the preparation of $LaVO_4$:Eu^{3+} nanophosphors.

Is there an increase in luminescence when the ratio of monoclinic to tetragonal phases increases in $LaVO_4$:Eu^{3+}? This has not been found in the literature to the best of authors' knowledge.

In this study, we have carried out the effect of codoping of uni-, bi-, and trivalent various metal ions (M^{n+} = Li^+, Sr^{2+}, and Bi^{3+}) on the luminescence and crystal structure in $LaVO_4$:Eu^{3+} NPs. Improvement in luminescence is found. Also, the effect of reaction medium is studied. For thin film optical devices, we have prepared polymer films.

2. EXPERIMENTAL SECTION

2.1. Synthesis of M^{n+} (M^{n+} = Li^+, Sr^{2+}, and Bi^{3+}) Codoped $LaVO_4$:Eu^{3+} Nanophosphors. The reagents were analytically pure and used without further purification. The precursors used were europium oxide (Eu_2O_3, 99.99% Aldrich), lanthanum oxide (La_2O_3, 99.99% Aldrich), ammonium metavanadate (NH_4VO_3, 99.99% Aldrich), lithium nitrate ($LiNO_3$, 99.99%, Aldrich), strontium nitrate ($Sr(NO_3)_2$, Merck), and bismuth nitrate ($Bi(NO_3)_3$, 99.99%, Aldrich). Ethylene glycol (EG, Merck, AR grade), water, and their mixed media were used as reaction medium.

Typically, for the preparation of 7 at. % of Eu^{3+} doped $LaVO_4$ codoped with 0.5 at. % Li^+, 0.5 g of La_2O_3, 0.04 g of Eu_2O_3, and 0.002 g of $LiNO_3$ were dissolved in minimum quantity of conc HCl in a 100 mL round-bottom flask and warmed to get a clear solution. The solution was evaporated at least three times by adding double distilled water so that excess HCl gets evaporated. Chlorides of La^{3+} and Eu^{3+} formed were mixed with 0.388 g of NH_4VO_3 and 50 mL of the solvent (water, EG, or EG + water). The pH of the solution was adjusted to 11 with 0.1 N NaOH and refluxed for 3 h at 140 °C (100 °C for samples prepared in water). The resulting colloidal solution was centrifuged at 10 000 rpm for about 10 min and washed two times with acetone and dried under ambient atmosphere. Here, 7 at. % of Eu^{3+} doped $LaVO_4$ is referred as $LaVO_4$:Eu. Similarly, M^{n+} = Li^+, Sr^{2+}, and Bi^{3+} codoped $LaVO_4$:Eu^{3+} nanophosphors were prepared.

2.2. Characterization. Crystal structure and phase purity of all the samples were studied using a powder diffractometer (PANalytical X'Pert Pro) in the 2θ range from 10° to 80°. The Cu Kα (λ = 1.5405 Å) radiation with a Ni filter was used. The average crystallite size (t) was calculated using Scherrer relation, $t = 0.9\lambda/(\beta \cos \theta)$ where λ is the wavelength of the X-ray and β is the full width at half-maximum (fwhm). The powder samples were ground and dispersed in methanol on a glass slide and allowed to dry.

The size distribution and morphology of the samples were studied using a Philips make CM-200 transmission electron microscope operating at an accelerating voltage of 200 kV. For this, the samples were ground and mixed together with EG and dispersed under ultrasonication for 30 min. A drop of dispersed sample was put over carbon coated copper grid and evaporated to dryness under IR lamp.

FTIR spectra of the $LaVO_4$ samples were studied using PerkinElmer Spectrum 400 FTIR spectrometer.

All the photoluminescence spectra were recorded using PerkinElmer (LS-55) luminescence spectrometer equipped with xenon lamp as the excitation source. The luminescence decays were recorded using Edinburgh Instrument FLS920 having microsecond flash lamps. A thin film of samples was spread on a thin glass slide with the help of methanol and dried before starting the reading.

3. RESULTS AND DISCUSSION

3.1. XRD Study. Figure 2 shows the X-ray diffraction (XRD) patterns of M^{n+} (= Li^+, Sr^{2+}, and Bi^{3+}) ion codoped $LaVO_4$:Eu^{3+} NPs prepared in EG medium. Every sample shows a mixture of tetragonal and monoclinic phases. $LaVO_4$ chemical formula can be considered as ABO_4. Let us consider concentration of "A" atoms as 100%. Here, Eu^{3+} concentration is fixed at 7 at. % with respect to A sites. Then M^{n+} ions are codoped with respect to (A-7) sites. Now, in the case of 7 at. % Eu^{3+}, substitution can take place on A sites because of similar ionic radii and similar chemical behavior. La^{3+} has 8 and 9 CN (CN = coordination number) in cases of tetragonal and monoclinic phases, respectively, and their corresponding ionic radii are 1.18 and 1.20 Å.[22] Eu^{3+} has 8 and 9 CN in cases of tetragonal and monoclinic phases, respectively, and the ionic radius of Eu^{3+} in 8 CN is 1.07. Now, can M^{n+} ions substitute (A-7) sites or not ?

Ionic size of M^{n+} = Li^+ is much lower than that of La^{3+}, and it prefers to have 4 and 6 CN, whereas La^{3+} prefers to have 6−11 CN. Ionic sizes of Li^+ with 4 and 6 CN are 0.59 and 0.74 Å, respectively. When Li^+ ions are codoped to $LaVO_4$:Eu, it is found that there is a shift in peak positions of tetragonal and monoclinic phases toward the lower 2θ in XRD pattern (Figure S1, see Supporting Information). On the basis of Bragg's law, it is expected to show the higher 2θ since ionic size of Li^+ is much less than La^{3+}. The spacing between the interplanner spacing (d_{hkl}) has a relationship with the Bragg's angle (θ) at constant X-ray wavelength (λ).

$$d_{hkl} = \lambda/(2 \sin \theta) \quad (1)$$

d_{200} (hkl = 200 of tetragonal phase) values of 0 and 3 at. % Li^+ codoped $LaVO_4$:Eu are 3.714 and 3.716 Å, respectively. It is suggested that Li^+ ions do not occupy La^{3+} sites. Instead, Li^+ ions occupy the interstitial sites of the lattice. A similar

dx.doi.org/10.1021/ic500828s | Inorg. Chem. 2014, 53, 7204−7213

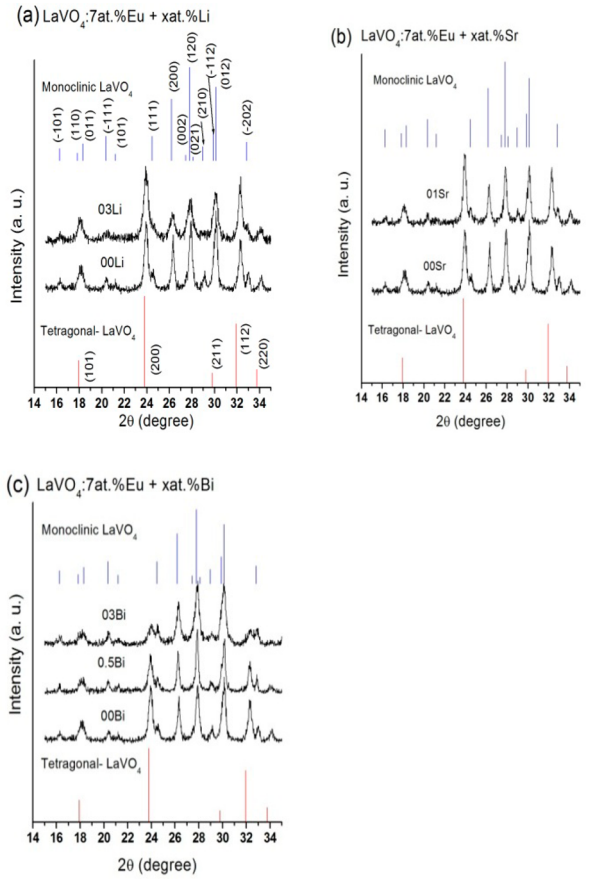

Figure 2. XRD patterns of $LaVO_4$:7 at. % Eu codoped with (a) Li, (b) Sr, and (c) Bi. To compare tetragonal and hexagonal phases of $LaVO_4$, standard XRD data (JCPDF 32-0504, 70-2392) are included.

observation has been reported in Li^+ codoped YPO_4:Eu.[23] There is an increase in ratio of tetragonal to monoclinic phases with Li^+ codoping as compared to that of $LaVO_4$:Eu. The crystallite size is calculated from the highest intensity peak in tetragonal phase. The crystallite sizes for $LaVO_4$:Eu^{3+} NPs without and with 3 at. % Li^+ codopant are found to be 24 and 18 nm, respectively.

M^{n+} = Sr^{2+} has higher ionic size than La^{3+}. Ionic size of Sr^{2+} based on 8 CN is 1.25 Å. It is expected to show peak shift to lower 2θ. This behavior is observed in XRD pattern (Figure S2, see Supporting Information). d_{hkl} values of 0 and 1 at. % Sr^{2+} codoped $LaVO_4$:Eu are 3.714 and 3.716 Å, respectively. However, there is a charge imbalance between Sr^{2+} and La^{3+}. There is an increase in ratio of tetragonal to monoclinic phases with Sr^{2+} codoping as compared to that of $LaVO_4$:Eu. The crystallite size for $LaVO_4$:Eu^{3+} NPs with 1 at. % Sr^{2+} codopant is found to be 29 nm.

M^{n+} = Bi^{3+} has lower ionic size than La^{3+}. Ionic size of Bi^{3+} based on 8 CN is 1.11 Å. It is expected to show peak shift to higher 2θ. This behavior is observed in XRD pattern (Figure S3, see Supporting Information). d_{hkl} values of 0 and 3 at. % Bi^{3+} codoped $LaVO_4$:Eu are 3.714 and 3.622 Å, respectively.

However, there is a charge balance between Bi^{3+} and La^{3+}. There is an increase in ratio of monoclinic to tetragonal phases with Bi^{3+} codoping as compared to that of $LaVO_4$:Eu. The crystallite size for $LaVO_4$:Eu^{3+} NPs with 3 at. % Bi^{3+} codopant is found to be 29 nm. Here crystallite size is calculated from the highest intensity peak (hkl = 120) in monoclinic phase.

Upon annealing up to 600 °C, we could not find variation of monoclinic to tetragonal phases in XRD patterns when compared to as-prepared samples of $LaVO_4$:Eu^{3+} codoped with M^{n+} (= 0, Li^+ and Bi^{3+}) ions. XRD patterns of 600 °C annealed samples are shown in Figure S4 (see Supporting Information).

The XRD patterns of Eu^{3+} (7 at. %) doped $LaVO_4$ NPs prepared in EG and water show the peaks corresponding to both monoclinic as well as tetragonal phases (Figure 3).

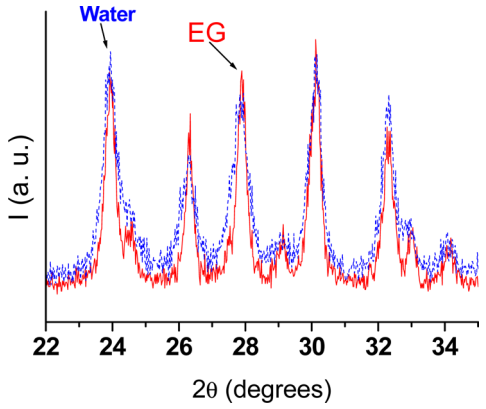

Figure 3. XRD patterns of $LaVO_4$:Eu^{3+} nanophosphors prepared in (a) EG and (b) water.

Notably, monoclinic structure is thermodynamically stable, whereas tetragonal structure is a metastable phase. It is found that when the solvent changes from EG to water, the ratio of tetragonal to monoclinic phases increases. There are few reports on such changes in tetragonal to monoclinic ratios with capping agent or pH.[20,24] The thermodynamic behavior of nanoscale particles depends on the free energy term γA which is defined as the product of the surface or interfacial free energy and the surface or interfacial area. When the surfaces of polymorphs of the same material possess different interfacial free energies, a change in phase stability can occur with decreasing particle size.[25,26] Here, we observed a change in the surface environment of the nanoparticles leading to the structural modification.

Strong polar water molecules orient to permit hydrogen and oxygen bonding to the terminating La^{3+} and VO_4^{3-} ions. Thus, strong interaction between water and the surface of the $LaVO_4$ NPs results in phase transformation. Variation of tetragonal to monoclinic phases in $LaVO_4$:Eu^{3+} nanophosphors prepared in EG (a) and water (b) along with codoping M^{n+} (= Li^+, Sr^{2+}, and Bi^{3+}) is shown in Figure 4.

3.2. TEM Study. Figure 5a shows the TEM image of 7 at. % Eu^{3+} doped $LaVO_4$ nanorods prepared in EG along with its selected area electron diffraction (SAED) pattern. Particle size distributions on the basis of diameter/breath and length are shown in Figure S5a (see Supporting Information). The particle size with 9 nm in diameter has the highest population, whereas that with 22 nm in length has the highest population. SAED pattern suggests the mixture of tetragonal and monoclinic phases.

The TEM image of 7 at. % Eu^{3+} doped $LaVO_4$ nanorods prepared in water is shown in Figure 5b along with the corresponding SAED pattern. Particle size distributions are shown in Figure S5b (see Supporting Information). Diameter and length of nanorods are found to be 11 and 20 nm,

dx.doi.org/10.1021/ic500828s | Inorg. Chem. 2014, 53, 7204−7213

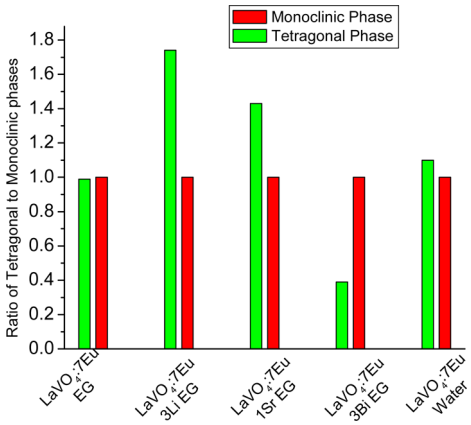

Figure 4. Variation of tetragonal to monoclinic phases in $LaVO_4:Eu^{3+}$ nanophosphors prepared in (a) EG and (b) water along with M^{n+} (= Li^+, Sr^{2+}, and Bi^{3+}) codoping.

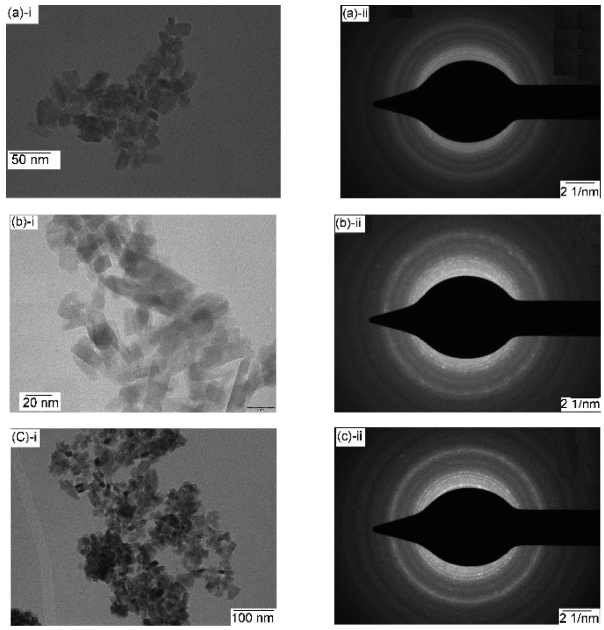

Figure 5. TEM images (left) for 7 at. % Eu^{3+} doped $LaVO_4$ in (a) EG and (b) water along with (c) Li^+ (3 at. %), 7 at. % Eu^{3+} doped $LaVO_4$ prepared in EG. Their corresponding SAED patterns are also shown (right).

respectively. SAED pattern suggests the mixture of tetragonal and monoclinic phases.

The TEM image of 3 at. % Li^+, 7 at. % Eu^{3+} codoped $LaVO_4$ nanorods prepared in EG gives length of 13 nm and diameter of 22 nm (Figure 5c, Figure S5c, see Supporting Information). The circular patterns in the SAED image (Figure 5c) reflect crystalline nature of the particles. A typical assignment of planes or reflections to SAED pattern is shown in Figure S6 (see Supporting Information). A mixture of tetragonal and monoclinic phases is found.

Energy dispersive analysis of X-ray (EDAX) spectra of three samples $LaVO_4$:7Eu; $LaVO_4$:7Eu, 3Li; and $LaVO_4$:7Eu, 3Bi are shown in Figure S7 (see Supporting Information). We have observed the presence of La, V, O, Eu, and Bi, but could not observe the presence of Li. Since Li is a light element, its atomic scattering factor is small. So, this is difficult to detect. Their nominal values are close to the calculated values (Table S1, see Supporting Information).

3.3. FTIR Study. The IR spectra of 7 at. % Eu^{3+} doped $LaVO_4$ nanophosphors synthesized in EG and water are shown in Figure S8 (see Supporting Information). Prominent peaks at 456, 777, 1385, 1596, 1636, 1649, 2846, 2927, and 3332 cm^{-1} are observed. Peaks at 1636 and 3332 cm^{-1} correspond to bending and stretching vibrations, respectively, for the O−H group of the EG molecule, which is used as a capping agent for nanoparticles.[27−31] The broad band at 3332 cm^{-1} therefore indicates the presence of a hydrogen bond in ethylene glycol molecules. Water associated with $LaVO_4$ could not be distinguished because the O−H peaks due to water have been merged with those of ethylene glycol. The peaks at 2846 and 2927 cm^{-1} correspond to the stretching vibrations of the CH_2 group of the ethylene glycol molecule. The peaks observed at 777 and 456 cm^{-1} are attributed to V−O vibrations of VO_4.[32] The peaks observed at 1385 cm^{-1} are related to scissoring (bending) vibration.[27]

3.4. Photoluminescence Study. The excitation spectra of $LaVO_4:Eu^{3+}$ coactivated with Li^+ ions (prepared in EG) monitoring emission at 615 nm are shown in Figure 6a. There are peaks below 250 nm, and these may be related to La−O charge transfer band (CTB).[33] A strong absorption band in 250−330 nm is observed. This is due to overlap of Eu−O and V−O CTB. Eu−O CTB will be at ∼260 nm.[18,19,33] The peaks at 280 and 310 nm will be related to V−O CTB because V−O can have 2 absorption bands. On the basis of molecular orbital theory, there are possible transitions from the $^1A_2$ ($^1T_1$) ground state to $^1A_1$ (^1E) and ^1E ($^1T_2$) excited states of VO_4^{3-} ion.[9] The charge transfer arises from the transition of 2p electrons of O^{2-} to the empty 3*d* orbitals of V^{5+} in VO_4 unit.[33] The 4f−4f absorption of the Eu^{3+} ions observed at 395 nm ($^7F_0 \rightarrow {}^5L_6$) is much weaker because of the low absorption cross-section and the forbidden character of the 4f transitions.[33] Upon monitoring emission at 615 nm of Eu^{3+}, a stronger absorption band is observed from VO_4 group as compared to Eu^{3+} (395 nm) indicating that there is energy transfer from VO_4 to Eu^{3+}.

When the metal ions (M^{n+} = Li^+, Sr^{2+}, and Bi^{3+}) are incorporated in $LaVO_4:Eu^{3+}$ matrix, the CTB corresponding to V−O/Eu−O in the UV region becomes more intense indicating that efficient energy transfer occurs in the systems. The intensity of the excitation band is maximum at 3 at. % for Li^+ codoped in $LaVO_4:Eu^{3+}$ samples, whereas 1 at. % Sr^{2+} and 3 at. % Bi^{3+} codoped samples give maximum intensity (Figure S9, see Supporting Information). Above these concentrations, the emission intensity decreases. The possible reason is that, at higher codoping concentrations, the distortion of crystal structure may occur due to large difference in ionic sizes (e.g., Li^+ and La^{3+}), charge imbalance (e.g., Li^+ and La^{3+}; Sr^{2+}, and La^{3+}), and difference in capability of coordination numbers (e.g., Li can have 4 or 6 CN and La can have 6−12 CN). This induces greater possibility that the transfer of the excited energy to quenching centers arose from distorted lattice at higher concentration of metal ions codoping.

Figure 6b shows emission spectra of $LaVO_4:Eu^{3+}$ with and without codoping of Li^+ (prepared in EG). Excitation wavelength is fixed at 280 nm (i.e., through VO_4 excitation). All the spectra show the characteristic emission peaks of Eu^{3+} doped in $LaVO_4$ matrix. The transitions corresponding to $^5D_0 \rightarrow {}^7F_{J=1,2,3,4}$ along with $^5D_1 \rightarrow {}^7F_1$, $^5D_2 \rightarrow {}^7F_2$, $^5D_3 \rightarrow {}^7F_2$ transitions were observed. Since the 4f energy levels of Eu^{3+} are

dx.doi.org/10.1021/ic500828s | Inorg. Chem. 2014, 53, 7204−7213

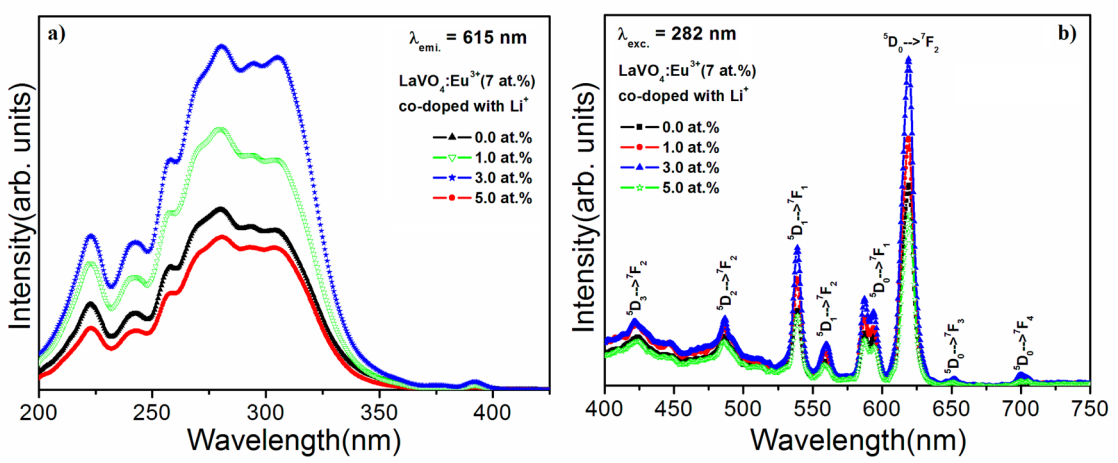

Figure 6. (a) Excitation spectra of $LaVO_4:Eu^{3+}$ (7 at. %) codoped with Li^+ ions monitoring emission at 615 nm and (b) emission spectra of $LaVO_4:Eu^{3+}$ (7 at. %) codoped with Li^+ ions excited at 282 nm. Samples are prepared in EG.

hardly affected by the crystal field,[33,34] no noticeable shift in the positions of the emission peaks is observed. From the emission spectra, $^5D_0 \rightarrow {}^7F_1$ transition is a magnetic dipole allowed transition, and its intensity is almost independent of the local environment around Eu^{3+} ions whereas the $^5D_0 \rightarrow {}^7F_2$ transition is an electric dipole allowed transition, which dominates over other transitions.[35,36] Eu^{3+} ions occupy La^{3+} sites with EuO_9 in the case of monoclinic structure and EuO_8 in the case of tetragonal structure of $LaVO_4$. There are 3 and 2 different bond lengths in EuO_9 and EuO_8 polyhedron, respectively.

EuO_9 and EuO_8 are highly asymmetric. Thus, it is expected that the electric dipole transition probability will be greater. This is happening in these compounds.

The presence of emission lines from higher excited state of Eu^{3+} ($^5D_1$, $^5D_2$, $^5D_3$) accounts to the low vibration energy of VO_4^{3-} groups (777 cm^{-1}). It arises as the multiphonon relaxation by VO_4^{3-} is not able to bridge the gaps between the higher energy levels ($^5D_1$, $^5D_2$, $^5D_3$) and $^5D_0$ level resulting in weak emissions from these levels.[18,19] Therefore, its intensity is sensitive to the local structure around Eu^{3+} ions. The $^5D_0 \rightarrow {}^7F_3$ transition exhibits a mixed magnetic dipole and electric dipole character. The $^5D_0 \rightarrow {}^7F_4$ is a forced electric dipole transition.

Further, the introduction of Li^+ ions leads to significant enhancement in emission intensity up to 3 at. % of Li^+ and then decreases with increase in Li^+ concentration. This mechanism of the effect of Li^+ on enhanced emission intensity has not yet been well-established, but it may be suggested that a low fraction of Li^+ ion doping in the lattice induces fast energy transfer from the host to Eu^{3+} ions and there is an increase in crystallinity.[23]

Increase in crystallinity gives a decrease of nonradiative rate that arose from defects, and thus, the probability of radiative transition increases. Moreover, once Li^+ attains a certain concentration (>3 at. % in this case), the defects or extra phase evolution in the host lattice greatly increases, and thus, it induces an increase of the nonradiative transition probability, leading to quenching in luminescence. Higher concentration of dopant gives rise to extra impurity.[23]

The emission intensity ratios of $^5D_0 \rightarrow {}^7F_1$ to the $^5D_0 \rightarrow {}^7F_2$ transitions of Eu^{3+} for $LaVO_4:Eu^{3+}$ as-prepared nanoparticles at various concentrations of Li^+ are shown in Figure 7 (prepared in EG). The ratio decreases up to 3 at. % of Li^+ codoped

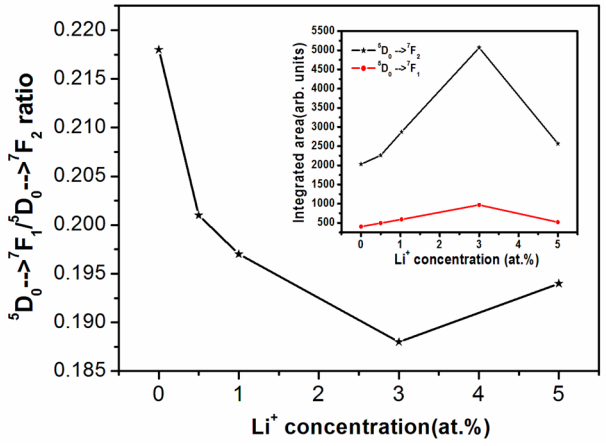

Figure 7. Emission intensity ratio of the $^5D_0 \rightarrow {}^7F_1$ peak to the $^5D_0 \rightarrow {}^7F_2$ peak vs Li^+ concentration. (Inset: Integrated area under the curve versus Li^+ concentration in $LaVO_4:Eu^{3+}$ matrix.) Samples are prepared in EG.

$LaVO_4:Eu^{3+}$ and then increases again. It is known that the $^5D_0 \rightarrow {}^7F_2$ transition is only possible when Eu^{3+} is embedded at a site of noninversion symmetry, while the $^5D_0 \rightarrow {}^7F_1$ transition is possible at a site with centrosymmetry.[36] Therefore, the fluorescence intensity of $^5D_0 \rightarrow {}^7F_1$ to $^5D_0 \rightarrow {}^7F_2$, known as the symmetry ratio, gives a measure of the degree of distortion from the inversion symmetry of the local environment surrounding the Eu^{3+} ions in the host matrix. The Eu^{3+} ion in monoclinic $LaVO_4:Eu^{3+}$ resides at a site with $P2_{1/n}$ space group;[21] therefore, the $^5D_0 \rightarrow {}^7F_2$ emission is more intense as compared to $^5D_0 \rightarrow {}^7F_1$ emission. However, since the introduction of Li^+ creates change in coordination number of Eu^{3+}, the symmetry strength of the local environment of Eu^{3+} will be undoubtedly reduced. It could be regarded that the incorporation of Li^+ ions in the host lattice will introduce a stress in the neighboring La^{3+} or Eu^{3+}.[37] Thus, the crystal field surrounding the Eu^{3+} ions would be altered. The sites offered for Eu^{3+} ions will have more reduced symmetry which is able to lift the parity selection rule and increase the transition probability of electron, resulting in prominent increase of emission intensity.[38]

dx.doi.org/10.1021/ic500828s | Inorg. Chem. 2014, 53, 7204−7213

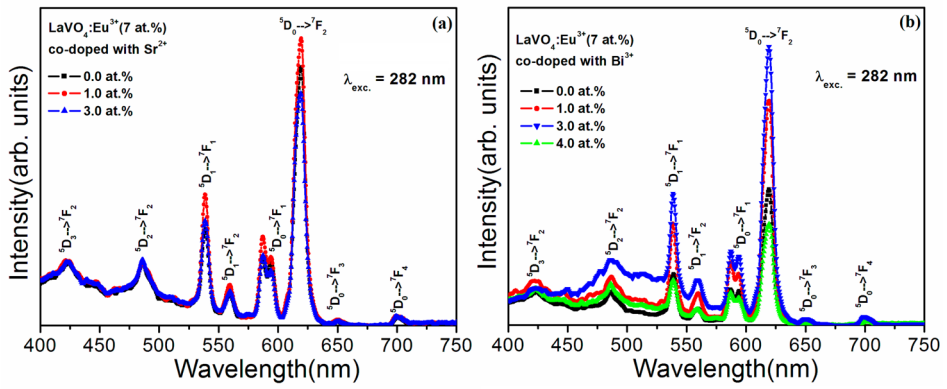

Figure 8. Emission spectra of $LaVO_4:Eu^{3+}$ (7 at. %) codoped with (a) Sr^{2+} and (b) Bi^{3+} ions excited at 282 nm. Samples are prepared in EG.

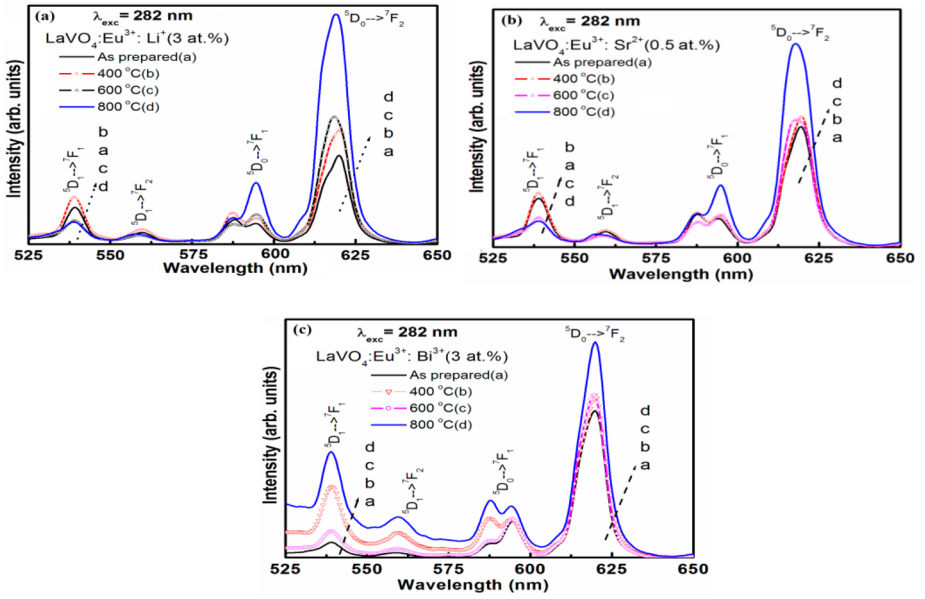

Figure 9. Comparative emission spectra of metal ion (M^{n+} = Li^+, Sr^{2+}, Bi^{3+}) codoped $LaVO_4:Eu^{3+}$ as-prepared as well as after annealing at 400, 600, and 800 °C upon excitation at 282 nm. Samples are prepared in EG.

The enhanced luminescence emission spectra for Sr^{2+} and Bi^{3+} coactivated $LaVO_4:Eu^{3+}$ NPs excited at 282 nm (Figure 8a,b) reached a maximum at 1 at. % and 3 at. %, respectively (prepared in EG). The increased intensity due to the incorporation of Sr^{2+} ions can be attributed to the increased absorption coefficient of the UV pump light or the enhanced luminescence efficiency by changing the composition and lattice parameters.[39−41] In the latter case, it may be related to the energy transfer from Bi^{3+} to Eu^{3+}. The excitation band of Bi^{3+} (338 nm) overlaps with the excitation band of $LaVO_4:Bi^{3+}$, Eu^{3+} (~282 nm). The 282 nm light excites both Bi^{3+} and VO_4^{3-} ions. The broad emission bands of Bi^{3+} (500−555 nm) and VO_4^{3-} ions (460 nm) are overlapping with absorption band of Eu^{3+} ($^7F_0 \rightarrow {}^5D_1$ and $^7F_0 \rightarrow {}^5D_1$), and thus, energy transfer can be favorable to the Eu^{3+} ion.[42] However, the transfer of energy is not prominent. The maximum transfer of energy from the sensitizer to an activator occurs when there is a spectral overlap of emission of the sensitizer and the excitation of an activator ion.

There is an enhancement in luminescence when ratio of tetragonal to monoclinic increases. This happens in cases of Li^+ and Sr^{2+} codoping systems prepared in EG and also samples prepared in water. But this is opposite to the Bi^{3+} codoping system in which there is enhancement in luminescence in spite of higher ratio of monoclinic to tetragonal. This is the first report to the best of the authors' knowledge. The enhancement in luminescence was reported in MVO_4 (M = Y, La) systems when the ratio of tetragonal to monoclinic increases.[43] Also, it was reported that Bi codoping enhances luminescence intensity in all tetragonal phase of YPO_4:Eu, Bi.[41] Also, it was reported that $BiPO_4$ would be good host due to higher absorption cross-section.[40]

In order to compare the emission intensity versus concentration of the codopant ions (Li^+), the integrated area under the curve of magnetic and electric dipole transition is calculated using Gaussian distribution function eq 2

$$I = I_B + \sum_{i=1}^{n} \frac{A_1}{w_i\sqrt{\frac{\pi}{2}}} e^{-2(\lambda-\lambda_{ci})^2/w_i^2} \quad (2)$$

where I is the intensity, I_B is the background intensity, w_i is the width at half-maximum intensity of the curve, and A_i is the area under the curve. λ is the wavelength, and λ_{ci} is the mean wavelength value corresponding to the transition. The highest emission intensity is observed at 3 at. % for Li^+ codoped $LaVO_4:Eu^{3+}$ NPs (Inset of Figure 7). The luminescence

dx.doi.org/10.1021/ic500828s | Inorg. Chem. 2014, 53, 7204−7213

emission intensity decreases with further increase in Li^+ ion concentration due to quenching effect.

3.5. Annealing Effect. Figure 9 shows the comparative emission spectra of metal ions (M^{n+} = Li^+, Sr^{2+}, Bi^{3+}) codoped $LaVO_4$:Eu^{3+} as-prepared samples (prepared in EG) as well as samples after annealing at 400, 600, and 800 °C upon excitation through the CTB of VO_4 at 282 nm. The emission spectra consist of sharp lines as expected for the transitions between f–f levels of Eu^{3+}, $^5D_0 \rightarrow {}^7F_{J=1,2}$. Apart from these peaks, we also observed emission peaks around 539 and 558 nm. These emission peaks correspond to the $^5D_1 \rightarrow {}^7F_{J=1,2}$ transitions from the higher excited state of $^5D_1$.[30,33]

From Figure 9 it is seen that the magnetic dipole $^5D_0 \rightarrow {}^7F_1$ transition is resolved into two peaks at ~586 and 594 nm due to Stark splitting while the hypersensitive $^5D_0 \rightarrow {}^7F_2$ transition is observed at ~619 nm. Generally, splitting depends on the following: (i) intensity of the exciting source, (ii) excitation/emission slit widths, and (iii) crystallinity. Increase of both i and iii and decrease of ii will split $^5D_{0,1} \rightarrow {}^7F_{J=1,2}$ transition.[33,44] However, splitting for Eu^{3+} emissions from $^5D_0 \rightarrow {}^7F_2$ could not be observed in our study. Reason for this is that we used low intensity of excitation source (150 W xenon lamps) and larger excitation/emission slit widths (5 nm) even though crystallinity of samples is high.

Emission intensity at ~594 and 620 nm decreases in the following order of annealing temperature 800, 600, 400 °C and as-prepared. The intensity of 800 °C heated sample is significantly higher than that of 600 °C heated sample. This may be attributed to the improvement in the crystallinity of the sample and the reduction of the surface defects resulting in decrease of the nonradiative transition probability. Up to 600 °C, there is no change in crystal structure (i.e., same as as-prepared samples).

In Figure 9a,b the peak positions of $^5D_1 \rightarrow {}^7F_{J=1,2}$ and $^5D_0 \rightarrow {}^7F_2$ transition exhibit blue shift with increase in annealing temperature. On close examination of the $^5D_0 \rightarrow {}^7F_1$ transition, the position of higher intensity peak changes from 587 to 594 nm with increase in annealing temperature in the case of Li^+ and Sr^{2+} codoped samples whereas the reverse has been observed for the 3 at. % Bi^{3+} codoped $LaVO_4$:Eu^{3+} samples (Figure 9c). It is expected that $^5D_0 \rightarrow {}^7F_1$ transition can have two transitions $j = 0 \rightarrow j = -1$ and $j = 0 \rightarrow j = 1$, but another transition $j = 0 \rightarrow j = 0$ is not allowed. Charges of Li^+ and Sr^{2+} are different from La^{3+} (host lattice), whereas charge of Bi^{3+} is the same as La^{3+}. It is concluded that such variation will be important in understanding charge imbalance and annealing after doping.

3.6. Effect of Solvents. The NPs of $LaVO_4$:Eu^{3+} (7 at. %) were synthesized in different reaction mediums such as EG, water, and their mixed media. Figure 10 represents the emission spectra of Eu^{3+} doped $LaVO_4$ NPs synthesized in these media after excitation at 282 nm. All the emission spectra show the same emission peaks at 615 nm (electric dipole transition, $^5D_0 \rightarrow {}^7F_2$) and at 593 nm (magnetic dipole transition, $^5D_0 \rightarrow {}^7F_1$). Interestingly, it is observed that the luminescence emission intensity is significantly enhanced for the NPs prepared in water compared to those prepared in other reaction media. Generally, the NPs prepared in water show lower luminescence intensity due to the presence of highly quencher group (OH) in the environment of the NPs.[24] In this study, enhancement in luminescence intensity in the case of a sample prepared in water is due to higher ratio of tetragonal to monoclinic phases. The similar observation was reported in $LaVO_4$:Eu^{3+}.[43] The

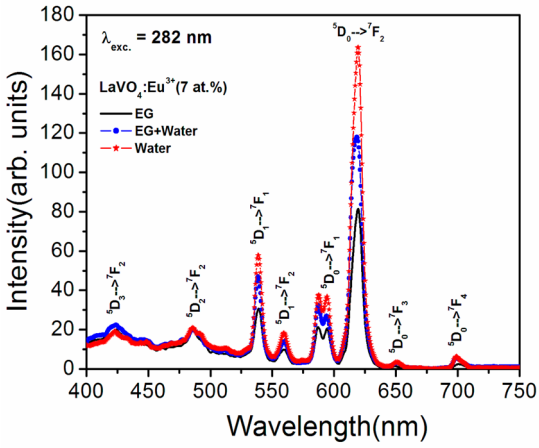

Figure 10. Emission spectra of $LaVO_4$:Eu^{3+} (7 at. %) NPs synthesized in different solvents (EG, water, and their mixture).

integrated area under the curve versus solvents used also corresponds to the observation that the emission intensity is highest for samples prepared in water (Figure S10, see Supporting Information).

3.7. Lifetime Study. The decays for $^5D_0$ level of Eu^{3+} are studied. Emission wavelength is fixed at 615 nm, and excitation wavelengths are fixed at 300 and 395 nm. At 395 nm excitation, Eu^{3+} ions absorb light and excited electrons at $^5L_6$ level come to $^5D_0$ level nonradiatively. Then decay starts. It follows a monoexponential decay equation.[9,33]

$$I = I_0 \exp(-t/\tau) \quad (3)$$

Here, I and I_0 are intensities at $t = t$ and $t = 0$, respectively.

Figure 11a shows decay curves of $LaVO_4$:Eu^{3+}, M^{n+} (= 0, Sr^{2+}, and Bi^{3+}) prepared in EG. The lifetime (τ) values for M^{n+} = 0, Sr^{2+} (1 at. %), and Bi^{3+} (3 at. %) are 0.08, 0.82, and 0.91 ms, respectively. It is suggested that lifetime is longer upon codoping of Sr^{2+} and Bi^{3+}. At 300 nm excitation (Figure 11b), host (VO_4^{3-}) absorbs light, and there is nonradiative energy transfer from V–O excited level to excited level of Eu^{3+}, and decay starts from the $^5D_0$ level. It follows a nonexponential decay equation.[44]

$$I = I_0 \exp(-t/\tau_1 - Dt^{0.5}) + \exp(-t/\tau_2) \quad (4)$$

D is related to diffusion and energy transfer. τ is lifetime for $^5D_0$ of Eu^{3+}. In the case of no codoping (M^{n+} = 0), D is found to be 1.26 $(ms)^{-0.5}$. τ_1 and τ_2 values are found to be 0.03 and 0.10 ms, respectively. For Sr^{2+} (1 at. %), D is found to be 0.12 $(ms)^{-0.5}$. τ_1 and τ_2 values are found to be 0.42 and 1.16 ms, respectively. For Bi^{3+} (1 at. %), D is found to be 0.30 $(ms)^{-0.5}$. τ_1 and τ_2 values are found to be 0.60 and 1.28 ms, respectively. It is suggested that lifetime values increase with codoping of M^{n+}, and its value is more for excitation through V–O CTB than that for direct excitation (395 nm).

Figure 11c shows decay curves for $^5D_0$ level of Eu^{3+} of sample $LaVO_4$:Eu^{3+} prepared in water after excitations at 300 and 395 nm. For excitation at 395 nm, the lifetime (τ) value after fitting with monoexponential is found to be 1.25 ms, which is more than that of the sample prepared in EG. For excitation at 300 nm, τ_1 and τ_2 values are found to be 1.71 and 1.65 ms, respectively, after fitting with eq 4. Inset of Figure 11c shows the comparison of decay curves for $^5D_0$ level of Eu^{3+} of sample $LaVO_4$:Eu^{3+} prepared in EG and water.

dx.doi.org/10.1021/ic500828s | Inorg. Chem. 2014, 53, 7204–7213

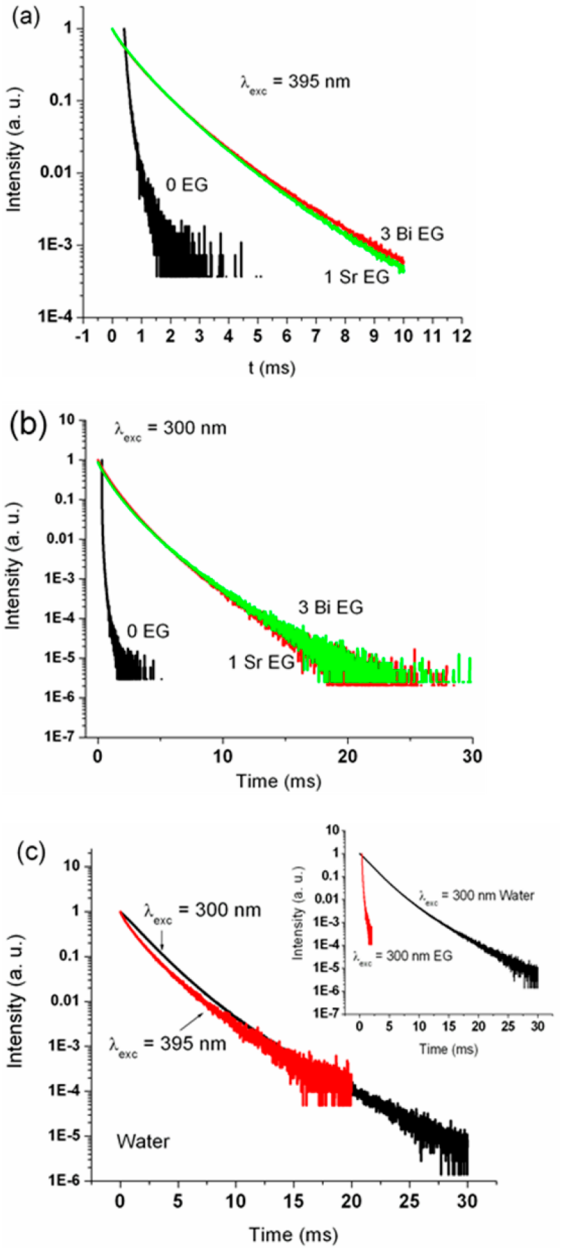

Figure 11. Decay curves for $^5D_0 \rightarrow {}^7F_2$ emission of Eu^{3+} in $LaVO_4$ matrix codoped with M^{n+} = 0, Sr^{2+}, and Bi^{3+} after excitation at (a) 395 and (b) 300 nm (samples are prepared in EG), and (c) those of sample ($LaVO_4$:Eu) prepared in water after excitation at 395 and 300 nm. Inset shows the decay curves for samples prepared in EG and water after excitation at 300 nm.

3.8. CIE Analysis. Figure 12 shows the Commission Internationale de l'Eclairage (CIE) chromaticity coordinates for $LaVO_4$:Eu^{3+} nanophosphors and those codoped with M^{n+} ions (prepared in EG). Eu^{3+} doped $LaVO_4$ nanophosphors have CIE coordinates of $x = 0.668$, $y = 0.298$. The M^{n+} ion codoped samples show better chromaticity for red emitter with the coordinates of $x = 0.672$, $y = 0.301$; $x = 0.670$, $y = 0.306$; and $x = 0.684$, $y = 0.312$ for Li^+, Sr^{2+}, and Bi^{3+}, respectively. It can be clearly seen that the codoping of M^{n+} gives deep-red emission with Li^+ codoping. Hence, these as-prepared samples are considered to be appropriate for deep-red-emitting phosphors that can further enhance the color rendering index (CRI).

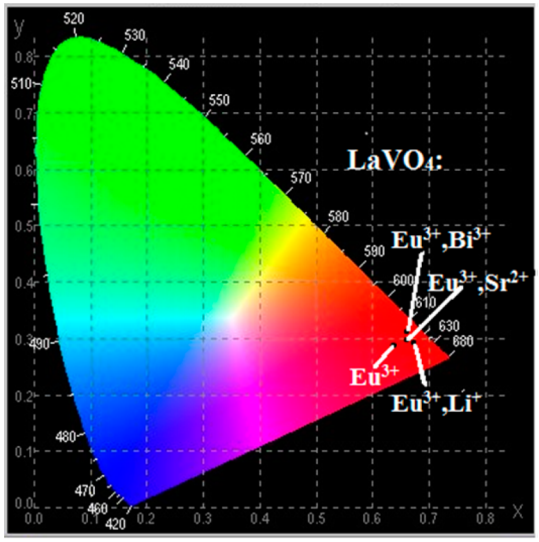

Figure 12. CIE chromaticity diagram for $LaVO_4$:Eu^{3+} nanophosphors and that codoped with M^{n+} ions. Samples are prepared in EG. Excitation is fixed at 280 nm.

3.9. Redispersion Study. We prepared films of PVA (poly(vinyl alcohol)) on the basis of the standard procedures.[45,46] The stock solutions of 5% PVA (poly(vinyl alcohol)) and 0.1 M borax (cross-linker) were prepared in double distilled water. A 5 mL portion of PVA stock solution was mixed with 10 mg of $LaVO_4$:Eu^{3+}, Li^+, and the mixture was subjected to ultrasonication for 1 h to get homogeneous dispersion. Concentrations of Eu^{3+} and Li^+ are fixed at 7 and 3 at. %, respectively. After sonication, 1.5 mL of borax solution was added to the mixture and stirred gently using a glass rod avoiding bubble formation. Slight heating at 50 °C was done so that homogeneous gel will be formed. The polymer gel formed is then transferred to a glass slide/Petri dish. A uniform film is obtained after keeping for 5 days at ambient atmosphere (Figure S11, see Supporting Information). Here, the PVA molecules are cross-linked by borax as depicted in Figure S12 (see Supporting Information). Also, VO_4^{3-} of $LaVO_4$:Eu^{3+}, Li^+ can interact with the OH group of the PVA.

The IR spectra of PVA, borax, and film (PVA + Borax +10 mg of $LaVO_4$:$7Eu^{3+}$, $3Li^+$) are shown in Figure S8 (see Supporting Information). In all spectra, 2352 cm^{-1} is observed, and this is related to CO_2/CO_3^{2-} (stretching) absorbed over particles.[27] The borax or borax−water has the following B−O−H vibration in 1000−1300 cm^{-1}, BO_3/BO_4 vibration in 700−1000 cm^{-1}, and O−B−O ring vibration in 400−700 cm^{-1}.[47] PVA has the vibrations of CH_2, O−H, and C−O. Film has the vibrations of CH_2, O−H, C−O, and V−O.

The redispersible properties of $LaVO_4$:Eu^{3+} codoped with Li^+ were investigated using polar solvent such as methanol as dispersion medium. Figure 13 shows the emission spectra of Li^+ codoped $LaVO_4$:Eu^{3+} sample prepared in EG. The characteristic emission peaks of Eu^{3+} are observed with $^5D_0 \rightarrow {}^7F_2$ being dominant in the spectra. The nanophosphors were also successfully incorporated in polymer film of PVA. The inset of Figure 13 shows the dispersion of the sample in methanol and red emission in polymer film after irradiation under UV light. Redispersion of the particles in the polar solvents is attributed to the presence of the O−H group on the surface of the prepared particles from the capping agent (EG). The presence of O−H group facilitates the formation of hydrogen

dx.doi.org/10.1021/ic500828s | Inorg. Chem. 2014, 53, 7204−7213

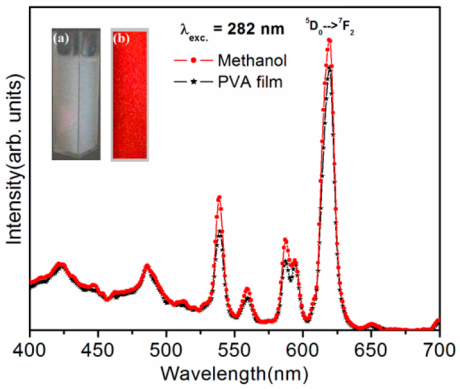

Figure 13. Emission spectra of Li^+ codoped $LaVO_4:Eu^{3+}$ nanophosphors. Inset shows the dispersion in methanol (a) and that incorporated in PVA film after irradiation under UV light (b).

bond with the polar solvents. Thus, nanophosphors are functionalized by EG. The redispersible capability of the samples may increase its application in biological assays, biological fluorescence labeling, etc. Also, polymer films could be potential phosphors for display devices.

Similarly, Ariga et al. developed multilayer films through layer-by-layer (LbL) assembly.[48] Guo et al. also reported conjugated polymers, which are useful in light emitting and solar cells.[49]

4. CONCLUSIONS

Crystalline $LaVO_4:Eu^{3+}$ nanophosphors codoped with metal ions, (M^{n+} = Li^+, Sr^{2+}, and Bi^{3+}) have been successfully prepared by using a polyol method. The ratio of monoclinic to tetragonal phases increases upon Bi^{3+} codoping, whereas this ratio decreases upon Li^+ and Sr^{2+} codoping when samples are prepared in EG medium. Ratio of tetragonal to monoclinic phases of $LaVO_4:Eu^{3+}$ increases when solvent changes from EG to water. Luminescence intensity is found to increase with M^{n+} codoping irrespective of crystal structure as well as with change in solvent from EG to water. The magnetic dipole transition ($^5D_0 \rightarrow {}^7F_1$) can have two transitions $j = 0 \rightarrow j = -1$ and $j = 0 \rightarrow j = 1$, and the intensity ratio of two transitions varies when 3+ charge of La^{3+} in $LaVO_4:Eu^{3+}$ is different from Li^+ (1+) and Sr^{2+} (2+) or the same as Bi^{3+} (3+). Lifetime is significantly longer in the case of M^{n+} codoping as compared to that without them. Improvement in luminescence is found upon annealing. Samples are dispersible in polar medium because of the presence of EG over particles, and stable polymer films are prepared. Samples show deep red emission.

■ ASSOCIATED CONTENT

Supporting Information

XRD patterns of metal ion (Li^+, Sr^{2+}, and Bi^{3+}) codoped $LaVO_4:Eu^{3+}$ nanophosphors prepared with EG. XRD patterns of 600 annealed samples of metal ion (Li^+, Sr^{2+}, and Bi^{3+}) codoped $LaVO_4:Eu^{3+}$ nanophosphors prepared with EG. EDAX and FTIR data. Excitation spectra of $LaVO_4:Eu^{3+}$ codoped with Sr^{2+} (a) and Bi^{3+} (b) ions monitoring emission at 615 nm. Luminescence integrated area under the curve versus reaction media for Eu^{3+} doped $LaVO_4$ nanophosphors. Images of polymer film and cross-link structure. This material is available free of charge via the Internet at http://pubs.acs.org.

■ AUTHOR INFORMATION

Corresponding Authors

*E-mail: rsn@barc.gov.in. Tel: +91 22 25592321. Fax: +91 22 25505151.

*E-mail: nrajmuhon@manipuruniv.ac.in. Tel: +91 94 36080780. Fax: +91 38 52435145.

Author Contributions

The manuscript was written through contributions of all authors. All authors have given approval to the final version of the manuscript.

Notes

The authors declare no competing financial interest.

■ ACKNOWLEDGMENTS

We greatly acknowledge SAIF, IIT, Bombay for assisting with TEM measurements. Two of the authors, N.R.S. and N.Y. acknowledge Department of Science and Technology (DST), New Delhi, for providing financial support during the execution of this work. R.S.N. thanks Dr. A. K. Parchur for drawing the scheme of Figure 1.

■ REFERENCES

(1) Levine, A. K.; Palilla, F. C. *Appl. Phys. Lett.* **1964**, *5*, 118−3.
(2) Yu, M.; Lin, J.; Wang, Z.; Fu, J.; Wang, S.; Zhang, H. J.; Han, Y. C. *Chem. Mater.* **2002**, *14*, 2224−2231.
(3) Maunders, E. A.; Deshaser, L. G. *J. Opt. Soc. Am.* **1971**, *61*, 648−697.
(4) Bass, M. *IEEE J. Quantum Electron.* **1975**, *11*, 938−941.
(5) O'Conner, J. R. *Appl. Phys. Lett.* **1966**, *9*, 407−3.
(6) Fields, R. A.; Birnbaum, M.; Fincher, C. L. *Appl. Phys. Lett.* **1987**, *51*, 1885−2.
(7) Fang, Z. M.; Hong, Q.; Zhou, Z. H.; Dai, S. J.; Weng, W. Z.; Wan, H. L. *Catal. Lett.* **1999**, *61* (1−2), 39−44.
(8) (a) Yi, G. S.; Lu, H. C.; Zhao, S. Y.; Yue, G.; Yang, W. J.; Chen, D. P.; Guo, L. H. *Nano Lett.* **2004**, *4*, 2191−2196. (b) Chen, Y. C.; Wu, Y. C.; Wang, D. Y.; Cheng, T. M. *J. Mater. Chem.* **2012**, *22*, 7961−7969.
(9) Singh, N. S.; Ningthoujam, R. S.; Yaiphaba, N.; Vatsa, R. K.; Singh, S. D. *J. Appl. Phys.* **2009**, *105*, 064303−7.
(10) (a) Okram, R.; Phaomei, G.; Singh, N. R. *Mater. Sci. Eng., B* **2013**, *178*, 409−416. (b) Krumpel, A. H.; Boutinaud, P.; Vander Kolk, E.; Dorenbos, P. *J. Lumin.* **2010**, *130*, 1357−1365.
(11) Shanta Singh, N.; Ningthoujam, R. S.; Phaomei, G.; Dorendrajit Singh, S.; Vinu, A.; Vatsa, R. K. *Dalton Trans.* **2012**, *41*, 4404−4412.
(12) Fan, W.; Bu, Y.; Song, X.; Sun, S.; Zhao, X. *Cryst. Growth Des.* **2007**, *7* (11), 2361−2366.
(13) Xie, B.; Lu, G.; Wang, Y.; Guo, Y.; Guo, Y. *Mater. Lett.* **2011**, *65*, 240−243.
(14) Palilla, F. C.; Levine, A. K.; Rinkevics, M. J. *J. Electrochem. Soc.* **1965**, *112*, 776−779.
(15) Rambabu, U.; Amalnerkar, D. P.; Kale, B. B.; Buddhudu, S. *Mater. Res. Bull.* **2000**, *35*, 929−936.
(16) Stouwdam, J. W.; Raudsepp, M.; van Veggel, F. C. J. M. *Langmuir* **2005**, *21*, 7003−7008.
(17) Jia, C. J.; Sun, L. D.; Yan, Z. G.; Pang, Y. C.; Lü, S. Z.; Yan, C. H. *Eur. J. Inorg. Chem.* **2010**, *18*, 2626−2635.
(18) Ningthoujam, R. S. *Pramana J. Phys.* **2013**, *80*, 1055−1064.
(19) Luwang, M. N.; Ningthoujam, R. S.; Srivastava, S. K.; Jaganath; Vatsa, R. K. *J. Am. Chem. Soc.* **2010**, *132*, 2759−2768.
(20) Chaochao, F.; Guangshe, L.; Minglei, Z.; Liusai, Y.; Jing, Z.; Liping, L. *Inorg. Chem.* **2012**, *51*, 5869−5880.
(21) Okram, R.; Singh, N. R.; Singh, Ak. M. *Micro Nano Lett.* **2011**, *6*, 165−169.
(22) Shannon, R. D. *Acta Crystallogr., Sect. A* **1976**, *32*, 751−767.
(23) Parchur, A. K.; Ningthoujam, R. S. *RSC Adv.* **2012**, *2*, 10854−10858.

(24) Phaomei, G.; Singh, W. R.; Ningthoujam, R. S. *J. Lumin.* **2011**, *131*, 1164−1171.
(25) Zhang, H.; Gilbert, B.; Huang, F.; Banfield, J. F. *Nature* **2003**, *424*, 1025−1029.
(26) McHalc, J. M.; Auroux, A.; Pcrotta, A. J.; Navrotsky, A. *Science* **1997**, *277*, 788−791.
(27) Nakamoto, K. *Infrared and Raman Spectra of Inorganic and Coordination Compounds*, 5th ed., Wiley: New York, 1986.
(28) Kemp, W. *Organic Spectroscopy*, 2nd ed., Macmillan: Hampshire, U.K., 1975.
(29) Gajbhiye, N. S.; Ningthoujam, R. S.; Ahmed, A.; Panda, D. K.; Umre, S. S.; Sharma, S. J. *Pramana J. Phys.* **2008**, *70*, 313−321.
(30) Ningthoujam, R. S.; Sudarshan, V.; Kulshreshtha, S. K. *J. Lumin.* **2007**, *127*, 747−756.
(31) Yaiphaba, N.; Ningthoujam, R. S.; Singh, N. R.; Vatsa, R. K. *Eur. J. Inorg. Chem.* **2010**, *18*, 2682−2687.
(32) Yamaguchi, O.; Mukaida, Y.; Shigeta, H.; Takemura, H.; Yamashita, M. *Mater. Lett.* **1988**, *7*, 158−160.
(33) Ningthoujam, R. S. *Enhancement of Luminescence by Rare Earth Ions Doping in Semiconductor Host*; Rai, S. B., Dwivedi, Y., Eds.; Nova Science Publishers Inc.: Hauppauge, NY, 2012; Chapter 7, pp 145−182.
(34) Ningthoujam, R. S. *Chem. Phys. Lett.* **2010**, *497*, 208−212.
(35) Ray, S.; Pramanik, P.; Singha, A.; Roy, A. *J. Appl. Phys.* **2005**, *97*, 094312−6.
(36) (a) Yaiphaba, N.; Ningthoujam, R. S.; Singh, N. S.; Vatsa, R. K.; Singh, N. R. *J. Lumin.* **2010**, *130*, 174−180. (b) Yaiphaba, N.; Ningthoujam, R. S.; Shanta Singh, N.; Vatsa, R. K.; Rajmuhon Singh, N. *J. Appl. Phys.* **2010**, *107*, 034301−9.
(37) Kaplyanskii, A. A.; Macfarlane, R. M. *Spectroscopy of Solids Containing Rare Earth Ions*; North-Holland: Amsterdam, 1987.
(38) Shi, S. K.; Gao, J.; Zhouf, J. *Opt. Mater.* **2008**, *30*, 1616−1620.
(39) Tian, L.; Mho, S. *J. Lumin.* **2007**, *122*, 99−103.
(40) Zhao, M.; Li, L.; Zheng, L.; Yang, L.; Li, G. *Inorg. Chem.* **2013**, *52*, 807−815.
(41) Luwang, M. N.; Ningthoujam, R. S.; Srivastava, S. K.; Vatsa, R. K. *J. Am. Chem. Soc.* **2011**, *133*, 2998−3004.
(42) (a) Pode, R. B.; Dhoble, S. J. *Phys. Status Solidi B* **1997**, *203*, 571−577. (b) Kim, C. H.; Park, H. L.; Mho, S. I. *Solid State Commun.* **1997**, *101* (2), 109−113. (c) Jacobsohn, L. G.; Blair, M. W.; Tornga, S. C.; Brown, L. O.; Bennett, B. L.; Muenchausen, R. E. *J. Appl. Phys.* **2008**, *104*, 124303−7.
(43) Jia, C. J.; Sun, L. D.; Yan, Z. G.; Pang, Y. C.; Lü, S. Z.; Yan, C. H. *Eur. J. Inorg. Chem.* **2010**, *18*, 2626−2635.
(44) Parchur, A. K.; Prasad, A. I.; Ansari, A. A.; Rai, S. B.; Ningthoujam, R. S. *Dalton Trans.* **2012**, *41*, 11032−11045.
(45) McLaughlin, K. W.; Wyffels, N. K.; Jentz, A. B.; Keenan, M. V. *J. Chem. Educ.* **1997**, *74*, 97−99.
(46) JCE Classroom Activity: *Chem. Lett.* **1998**, *75*, 1432A−1432B.
(47) Peak, D.; Luther, G. W.; Sparks, D. L. *Geochim. Cosmochim. Acta* **2003**, *67*, 2551−2560.
(48) Ariga, K.; Yamauchi, Y.; Rydzek, G.; Ji, Q.; Yonamine, Y.; Wu, K. C. W.; Hill, J. P. *Chem. Lett.* **2014**, *43*, 36−68.
(49) Guo, X.; Baumgarten, M.; Mullen, K. *Prog. Polym. Sci.* **2013**, *38*, 1832−1908.